Radiochim. Acta **88**, 657–664 (2000)

Uranium(VI) and neptunium(V) transport through fractured, hydrothermally altered concrete

By S. L. Matzen[1], J. M. Beiriger[2], P. C. Torretto[2], P. Zhao[3] and B. E. Viani[1,*]

[1] Geosciences and Environmental Technologies Division, Lawrence Livermore National Laboratory, L-219, Livermore, California 94550, USA
[2] Analytical & Nuclear Chemistry Division, Lawrence Livermore National Laboratory, L-219, Livermore, California 94550, USA
[3] G.T. Seaborg Institute for Transactinium Science, Lawrence Livermore National Laboratory, L-219, Livermore, California 94550, USA

(Received November 8, 1999; accepted April 3, 2000)

Uranium(VI) / Neptunium(V) / Sorption / Cementitious material / Colloid / Microsphere / Alpha particle tracks / SIMS

Summary. In a high level waste repository in which temperatures are elevated due to waste decay, concrete structures will be subjected to hydrothermal conditions that will alter their physical and chemical properties. Virtually no studies have examined the interaction of hydrothermally altered concrete with radionuclides. We present the results of experiments in which soluble and colloid-associated U and Np, were eluted into a fractured, hydrothermally altered concrete core. Although the fluid residence time in the fracture was estimated to be on the order of 1 minute, U and Np in the effluent from the core were below detection (10^{-9}–10^{-8} M), for both soluble and colloid-associated species. Inorganic colloids and latex microspheres were similarly immobilized within the core. Post-test analysis of the core identified the immobilized U and Np at or near the fracture surface, with a spatial distribution similar to that of the latex microspheres. Because hydrothermal alteration followed fracturing, the growth of crystalline calcium silicate hydrate and clay mineral alteration products on, and possibly across the fracture, resulted in a highly reactive fracture that was effective at capturing both soluble and colloidal radionuclides. Comparison of results from batch experiments [1] with these experiments indicate that partitioning of U and Np to the solid phase, and equilibration of the incoming fluid with the concrete, occurs rapidly in the fractured system. Transport of U through the concrete may be solubility and/or sorption limited; transport of Np appears to be limited primarily by sorption.

Introduction

Concrete will play an important role in controlling radionuclide releases from many prospective nuclear waste repositories. Radionuclide interactions with concrete have been investigated primarily in the context of low-level waste isolation and/or ambient-temperature high-level waste repositories [2, 3]. However, virtually no studies have addressed the interaction between radionuclides and concrete that has been altered by exposure to high temperatures generated by waste decay, such as may occur in the potential repository at Yucca Mountain, NV. We present the results of experiments in which soluble and colloid-associated actinides, uranium (U) and neptunium (Np), were eluted into a fractured, hydrothermally altered concrete core.

In a related study, Zhao *et al.* [1] report partition coefficients for U and Np on the order of 10^3 to 10^5 mL/g for crushed ($< 53\,\mu$m) samples of hydrothermally altered concrete identical to the concrete used in this study. Partition coefficients were approximately an order of magnitude greater in filtered samples than in unfiltered samples, indicating significant sorption onto suspended particles.

A goal of this study was to determine if U and Np partitioning on crushed concrete is replicated during transport through fractured concrete, a medium expected to more closely approximate concrete in a repository setting. Given the potential for radionuclide transport via colloids, we studied the transport of U and Np in dissolved form as well as associated with colloidal particles derived from the concrete.

Methods

Materials

The concrete used in this study was cored from pre-cast concrete inverts (ordinary Portland cement with a dolomitic limestone aggregate) used in the Yucca Mountain Project's (YMP) Exploratory Studies Facility, Yucca Mountain, NV. A single fracture was induced in a cylindrical core using an hydraulic press, and the two halves were secured together with Teflon™-coated wire. The core was placed in a 316 stainless steel hydrothermal reaction vessel, submerged in 3×10^{-3} M $NaHCO_3$, and reacted at 200 °C for 8 months. The treated core was trimmed to a cylinder 5.40 cm long and 5.08 cm in diameter and the edges sealed with silicone to prevent fluid from bypassing the core.

By assuming all flow through the core was transmitted through the fracture, the pressure difference between the up- and downstream core faces, and the flow rate through the core were used to calculate the aperture of an equivalent

*Author for correspondence (E-mail: viani@llnl.gov).

rectangular fracture. The average aperture height (based on 12 transport experiments) was $\sim 6\,\mu m$, which corresponds to a fracture volume of 0.016 mL. In contrast, the total connected porosity of the core matrix was calculated to be 0.20 (21.9 mL) by comparing the water saturated weight to the oven dry (52 °C) weight.

Concrete characterization

The mineralogy of the unaltered and hydrothermally altered concrete was identified by X-ray diffraction analysis (XRD) using a Scintag X-ray diffractometer with Cu K_α radiation. Bulk samples of ground concrete were X-rayed using a side-mount sample holder. Clay-sized particles ($< 1\,\mu m$) were separated by centrifugation, washed with $MgCl_2$ to saturate exchange sites and flocculate the clay, washed with deionized water, and deposited as oriented films on zero-background quartz plates. The oriented films were solvated with ethylene glycol to assist in identification of layer silicate clays.

Minerals identified in the unaltered and hydrothermally altered concrete are shown in Table 1. During hydrothermal treatment, portlandite ($Ca(OH)_2$), quartz, and amorphous calcium-silicate-hydrate gels altered to the crystalline Ca-Si-H_2O phases scawtite ($Ca_7Si_6(CO_3)O_{18}$-$2H_2O$), tobermorite ($Ca_5Si_5(OH)_2$-$4H_2O$) and xonotlite ($Ca_6Si_6O_{17}(OH)_2$). In addition, hydrothermal treatment also resulted in the formation of two clay minerals, smectite, a 2 : 1 layer silicate clay, and serpentine, a 1 : 1 layer silicate.

Transport experiments

The core was encased in a Viton™ rubber sleeve, fixed between two Teflon™ fluid distribution plates, and inserted in the core-flow apparatus (Fig. 1). A confining pressure of $\sim$ 3.4 MPa was applied to the Viton-encased core via a hydrocarbon fluid (Isopar™) to prevent fluid flow along the outside of the core. The confining pressure cycled (± 0.3 MPa) in response to diurnal temperature changes (± 0.5 °C).

A piston pump was used to elute a carrier solution of 0.01 M NaCl at constant flow rate. Tracer and sample solutions were input into the carrier solution through sample injection loops (0.50, 5.00, and 11.69 mL) upstream from the core. Effluent from the core was collected using a drop-counter fraction collector. Upstream and downstream fluid pressure, confining fluid pressure, and core temperatures were continuously monitored using pressure transducers and thermocouples. The transport experiments are summarized in chronological order in Table 2.

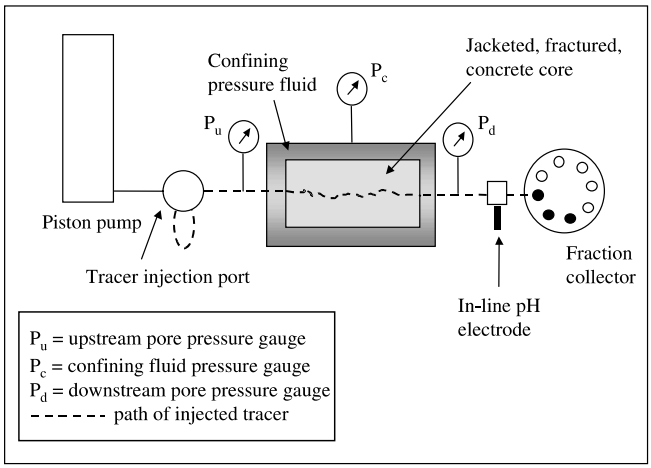

Fig. 1. Schematic of fracture flow apparatus.

Fluid analysis

Effluent samples were analyzed for iodide using an iodide selective electrode, for U and Np using liquid scintillation, for cationic constituents and silica using inductively coupled plasma atomic emission spectrometry (ICP-AES), for anions using ion chromatography, for dissolved inorganic carbon using titration, for inorganic colloids using laser breakdown spectrometry (LBS), and for colloidal microspheres using fluorimetry. Uranium solutions were 98.45 mass percent ^{238}U, 0.85 mass percent ^{233}U, and 0.65 mass percent ^{235}U, as determined by thermal ionization mass spectrometry and alpha spectroscopy, and standardized against NIST U using UV-VIS spectroscopy. The ^{237}Np stock solution was standardized using a NIST-calibrated gamma spectroscopic standard; the ^{233}Pa daughter was a negligible percentage of total radioisotope mass. The oxidation states of Np(V), and U(VI), were verified using UV-VIS spectroscopy.

Concrete-derived colloids

Concrete-derived colloids were prepared by separating the < 1-μm fraction from crushed concrete by successive rounds of ultra sonic dispersion followed by centrifugation. The colloids were identified (via XRD) to be primarily calcite and smectite. The particle size distribution of the colloids suspended in 0.01 M NaCl was determined to be monomodal, with an average particle diameter of 320 nm, based on analysis with photon correlation spectrometry.

Particle concentrations in the effluent were assayed using LBS, which detects the acoustic wave emitted when a laser beam interacts with a particle [4]. Although absolute concentrations or particle size data could not be measured, the detection limit based on 496 nm polystyrene standards was conservatively estimated to be $\sim 10^6$ particles/mL.

Table 1. Mineral phases identified by X-ray diffraction in untreated and hydrothermally treated concrete.

Phase	Untreated concrete	Hydrothermally treated concrete
Dolomite	major[a]	major
Calcite	major	major
Quartz	major	minor
Portlandite	major	not observed
Scawtite	not observed	minor
Tobermorite	not observed	minor
Xonotlite	not observed	minor
Smectite	not observed	minor
Serpentine	not observed	minor

a: *Major*, *minor* indicates relative abundance of the phase based on XRD peak heights.

Table 2. Chronological summary of fracture flow experiments.

Test ID[a]	Carrier fluid/eluent	Injected tracer	Tracer concentration	Pulse volume (mL)	Total effluent collected[b] (mL)	Tracer detection limit	Flow rate (mL/hr)	Average permeability (10^{-16} m^2)
I-111397	0.01 M NaCl, pH 6	Iodide	7.5×10^{-4} M	0.56	65	5×10^{-8} M	1	9.12
I-121997	0.01 M NaCl, pH 6	Iodide	7.5×10^{-4} M	0.56	86.5	5×10^{-8} M	1	3.65
Np-123197	0.01 M NaCl, pH 6	Dissolved Np	2.6×10^{-6} M	5.06	189	8×10^{-9} M	1	4.66
U-010998	0.01 M NaCl, pH 6	Dissolved U	2.1×10^{-6} M	5.06	218	1×10^{-8} M	1	6.75
I-072298	0.01 M NaCl, pH 6	Iodide	7.5×10^{-4} M	0.56	114	5×10^{-8} M	1	4.24
CC-092898	0.01 M NaCl, pH 6	Concrete colloids	371 mg/L	11.75	40	4×10^{-2} mg/L	1	6.51
NpS-100298	0.01 M NaCl, pH 6	Dissolved Np	2.0×10^{-6} M	11.75	91	2×10^{-9} M	1	6.01
NpC-100798	0.01 M NaCl, pH 6	Np-spiked colloids	157 mg/L	11.75	34	2×10^{-8} M Np; 4×10^{-2} mg/L particles	1	5.82
NpC-102698	0.01 M NaCl, pH 6	Np-spiked colloids	157 mg/L	11.75	56	4×10^{-9} M Np; 4×10^{-2} mg/L particles	1	4.42
I-111298	0.01 M NaCl, pH 6	Iodide	7.5×10^{-4} M	0.56	22	5×10^{-8} M	1	4.32
I-111698	0.01 M NaCl, pH 6	Iodide	7.5×10^{-4} M	0.56	15.5	5×10^{-8} M	0.1	4.01
C-112598	2 mM HCO_3^-, pH 8.46	(none)	–	–	535	6×10^{-8} M U; 8×10^{-9} M Np	1[c]	2.48
M-122198	0.01 M NaCl, pH 6	Microspheres	4.5×10^7 particles/mL	5.06	16	400 particles/mL	1	1.94

a: Test ID indicates date of test (MMDDYY).
b: Total effluent collected after tracer pulse injected into flow.
c: Flow rate was changed to 0.1 mL/hr for the last 7 mL of effluent collected.

Np-associated colloids

Transport experiments (Table 2) were conducted with untraced and Np-spiked colloid suspensions. The spiked suspension was prepared by adding a small amount (11 μL) of NpO_2^+ stock solution to the suspension (total Np $\sim 2 \times 10^{-6}$ M), along with NaOH to maintain the pH of the suspension at 9. Neptunium partitioning to the colloids determined by counting filtered and unfiltered samples varied between 30%–50% of the Np added. The suspension was monitored several times during each experiment to verify that there were no changes in Np partitioning.

Fluorescent microspheres

One transport test (Table 2) was done using 1-μm fluorescent Fluoresbrite™ carboxylate microspheres. The lower detection limit, using fluorimetry, was conservatively estimated to be 400 particles/mL.

Post-experiment core analysis

Following the transport experiments, the core was removed from the apparatus and analyzed. Scanning electron microscopy was used to examine minerals on the fracture surface and the up- and downstream faces of the core. To gauge the extent of radionuclide transport along the fracture and into the matrix, alpha particle tracks were recorded in film (TASTRAK CR-39[1]) exposed to thin sections cut from the core (Fig. 2a) [5]. In addition, the relative concentrations of U and Np along a transect from the fracture into the matrix was measured using a Cameca IMS 3F secondary ion mass spectrometer (SIMS) using methods developed previously for rock and glass samples [6, 7]. The SIMS measurements were made on a thin section cut from the upstream face of the core (Fig. 2a).

Geochemical modeling

Geochemical modeling was used to assess potential solubility controls on U and Np partitioning in concrete. Solution speciation and mineral equilibria were calculated using the geochemical modeling code REACT [8] and version thermo.com.full.V8.R6 of the GEMBOCHS thermodynamic database [9]. It was assumed that the system was oxidizing (fugacity $O_2 = 0.2$) and, for non-carbonate containing carrier solutions, that the fugacity of CO_2 was controlled by dissolution and equilibration with calcite.

[1] Obtained from Track Analysis Systems, Ltd., Bristol, U.K.

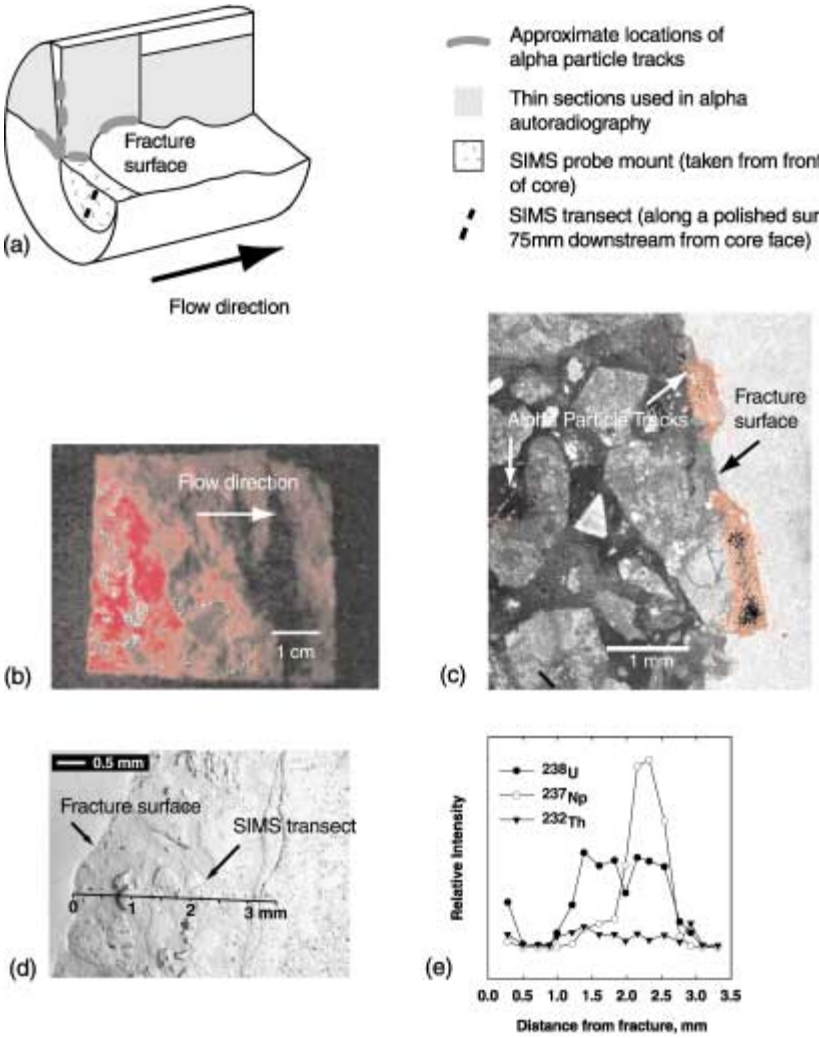

Fig. 2. Post-test examination of the fractured concrete core. The core was separated along the fracture surface, and the upper half was sawn in two longitudinally. (**a**) Diagram showing cut concrete core and analysis locations. The entire lower half of the core fracture surface was photographed to show positions of fluorescent microspheres. Thin sections cut along the front and longitudinal faces from one of the upper core pieces were used for alpha track autoradiography. A section cut from the front surface of the lower half of the core, was polished (removing $\sim$ 50–75 μm), and used for the SIMS analysis. (**b**) Photograph of lower fracture surface showing immobilized fluorescent latex microspheres (bright areas). (**c**) Alpha particle tracks (red) superimposed on an optical micrograph of a thin section taken from the vertical surface of the longitudinal saw-cut showing the fracture surface. Material to right of fracture surface is epoxy. (**d**) SEM micrograph showing SIMS transect. Material to left of fracture surface is epoxy. (**e**) Relative radionuclide concentrations along SIMS transect.

Results and discussion

Carbonation of concrete

A major chemical/mineralogical alteration expected in concrete exposed to groundwater is 'carbonation'; the growth of calcite at the expense of relatively soluble 'cement' phases such as portlandite and amorphous calcium silicate hydrate (CSH) gels. Hydrothermal alteration of these phases to more crystalline CSH phases would be expected to significantly affect both the rate and extent of carbonation of concrete. The extent of carbonation and its effect on concrete/radionuclide interaction would depend on the relative timing of radionuclide release and hydrothermal alteration. The concrete used in this study contained abundant calcite and dolomite introduced in the aggregate; hence, the results presented are most relevant to radionuclide interaction with a hydrothermally altered concrete that has been significantly carbonated.

Distribution of alteration products in core

Scanning electron microscope (SEM) images of the core show complex alteration of the fracture surface and the up- and downstream core faces (Fig. 3). The fracture surface is covered with blade-like, fibrous, and platy alteration products (Figs. 3a,b). Based on morphology, the blade-like and fibrous structures are tentatively identified as Ca-Si-H_2O phases, and the platy minerals are tentatively identified as clays. SEM analysis of pieces of altered concrete not subjected to the eluents used in this experiment showed similar alteration products. Therefore, we assume that these phases formed during the hydrothermal alteration of the core, not during the fracture flow experiments. However, acicular alteration products observed on the downstream end were not observed on the upstream face (Figs. 3c,d). It is possible that the acicular phase has been dissolved from the upstream face during flow tests by the large volume of pH 6 NaCl carrier solution ($\sim$ 500 mL) and/or the pH $\sim$ 4 radionuclide tracer solutions ($\sim$ 20 mL) that were pumped through the core. Alternately, this phase may represent an alteration product that formed on the down-stream face during flow-testing.

Effluent composition

The composition of the effluent is listed in Table 3 and compared to the composition of fluids determined after equilibration of crushed concrete in batch tests [1]. The pH as measured with in-line electrodes was 11.2, about 0.5 unit higher than in the batch experiments and the calcium levels were also larger in the effluent vs. the batch tests. The contact times in the batch experiments were on the order of months. In contrast, at a flow rate of 1 mL/hr, the residence

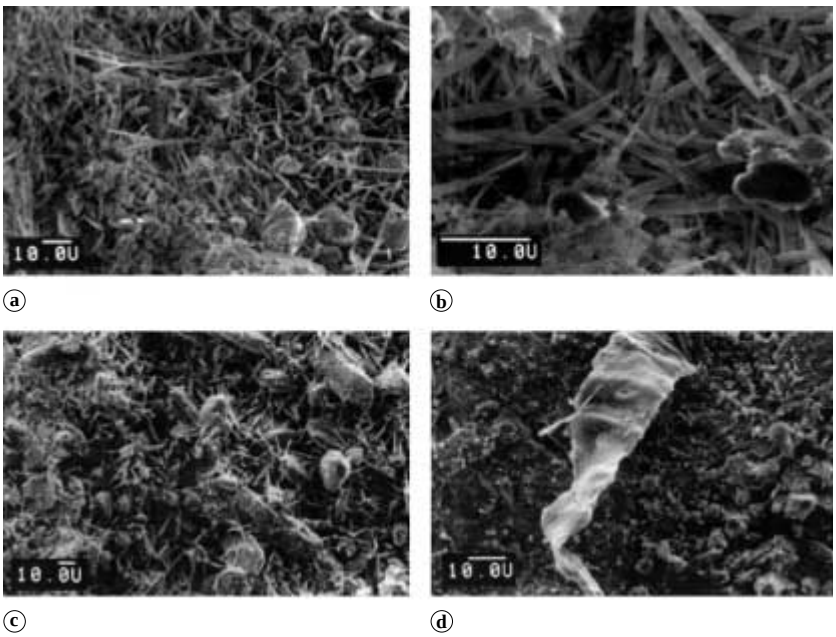

Fig. 3. SEM images of hydrothermally altered fractured concrete core; (**a**) and (**b**) micrographs of fracture surface; (**c**) micrograph of upstream face of core; (**d**) micrograph of downstream face.

time in the fracture (based on an effective fracture volume of 0.016 mL) is $\sim$ 1 minute. The assumption that equilibrium with calcite could control dissolved carbonate levels was tested using the React geochemical modeling code [8]. Although the residence time is small, because of the relatively large ratio of fracture surface area to fracture volume, calculations using React, with explicit consideration of calcite dissolution kinetics at pH 11 [10], show that equilibrium with calcite would be obtained within 1 minute for reasonable calcite surface areas (e.g., $> 0.2\times$ the geometric surface area of a rectangular fracture). Therefore, in the absence of an external source of CO_2 (aside from that introduced with the 0.01 M NaCl carrier solution), dissolved carbonate levels are predicted to be small (< 1.5 mg/L C) when controlled by calcite equilibrium. The difference in dissolved calcium between batch and flow tests, may arise because the batch tests were equilibrated in the absence of CO_2 (under argon) [1], and would be expected to equilibrate at a significantly lower concentration of dissolved carbon than in the flow tests. Apparently, the reaction of Si-bearing phases with the eluent is rapid as well, because the dissolved Si concentration in effluent and batch tests is similar.

Table 3. Compositions of fluid[a] in contact with hydrothermally altered concrete.

	Core Effluent[b] (mg/L)	Batch Fluid[c] (mg/L)
Ca[d]	39.1	23
Mg	0.1	< 0.5
K	0.5	10[g]
Na	227	230[h]
Si	8.66	8.6
Sr	0.23	0.065
Cl[e]	367	355[h]
SO_4	18.3	Not analyzed
pH[f]	11.2	10.7

a: Carrier/eluent solutions are shown in Table 2.
b: Average composition of effluent from fracture flow experiments.
c: From batch sorption experiments Zhao *et al.* [1].
d: Cations analyzed with ICP-AES.
e: Anions analyzed with ion chromatography.
f: pH of core effluent measured with in-line electrode; pH of batch fluid measured with standard electrode.
g: Contaminated by KCl from pH electrode.
h: Assumed based on 0.01 M NaCl supporting electrolyte.

Transport of iodide

Iodide transport through soils and sediments is generally non-retarded and conservative [11], although partitioning of iodide to fresh Portland cement has been documented [12–14]. Integration of the iodide breakthrough curves (Figs. 4a,b) yielded recoveries that depended on volume of the effluent collected (Fig. 4c). The data in Fig. 4c suggest that all five iodide tests behave similarly; essentially complete recovery is indicated for elution volumes greater than $\sim$ 50 mL. Recoveries $> 100\%$ reflect a combination of background iodide, and/or carry over of iodide from prior tests. These data suggest that transport of iodide through concrete is conservative, as observed previously for an identically sized core of welded volcanic tuff containing a 25-μm saw-cut fracture [15]. The initial appearance of iodide in the effluent begins 3–4 mL following injection, similar to that observed for the saw-cut welded volcanic tuff using the same apparatus (Fig. 4b). Therefore, for the core length and flow rates used in these experiments, there is no measurable retardation of iodide relative to a volcanic tuff.

The breakthrough curve for iodide eluted at 0.1 mL/hr is broader and more diffuse than those at 1 mL/hr, but the initial appearance of iodide is similar (Fig. 4b). This suggests that diffusion of iodide into the matrix during the passage of the pulse, and its subsequent diffusion from the matrix to the fracture is more pronounced at low flow ($\sim$ 0.5 hour for a 0.56-mL pulse to traverse the fracture at 1 mL/hr; and $\sim$ 5 hours at 0.1 mL/hr). Matrix diffusion appears to exert a greater effect on breakthrough curves in this concrete compared to the low porosity volcanic tuff studied previously

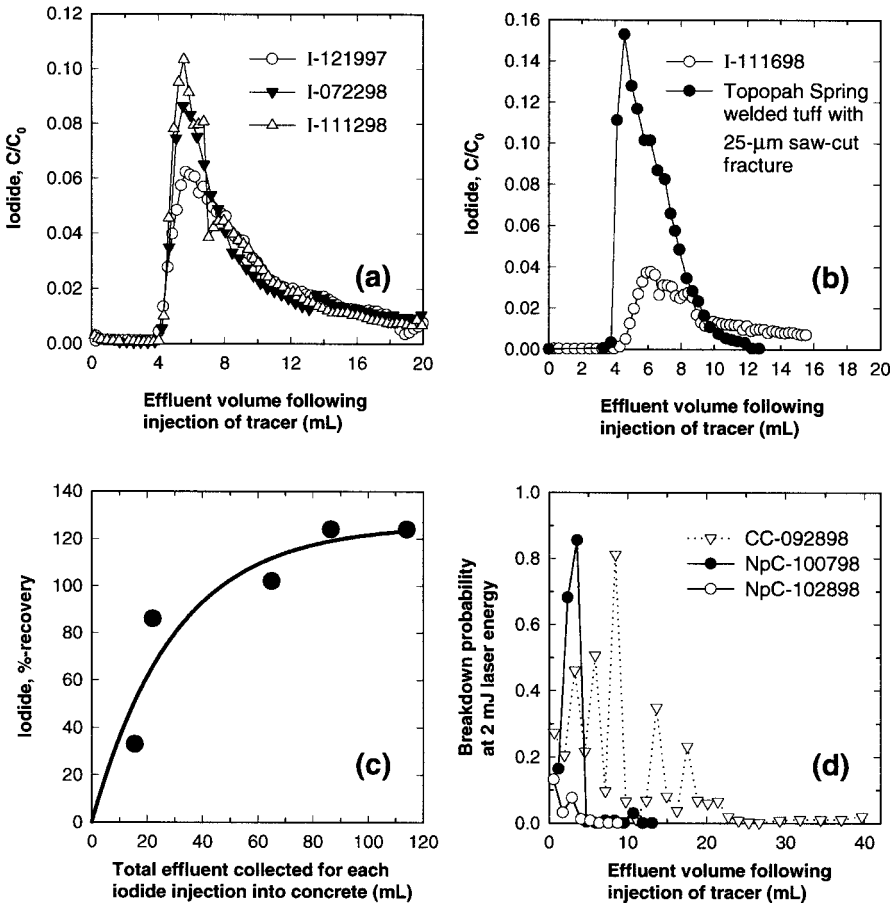

Fig. 4. Elution of iodide and concrete-derived colloids; (**a**) breakthrough curves for iodide injected into concrete core (1.0 mL/hr); (**b**) breakthrough curves for iodide injected into concrete and volcanic tuff cores (0.1 mL/hr); (**c**) recovery of iodide from five separate iodide injections into concrete core; (**d**) breakthrough curves for concrete-derived colloids injected into concrete core (1.0 mL/hr). Transport experiment identifiers are listed in Table 2.

(Fig. 4b). Because of the slow flow rate, only 15 mL of effluent were collected, hence the recovery was only 33%.

Latex microspheres

The movement of fluorescent latex microspheres through the core, as seen in a photograph of the fracture surface (Fig. 2b), indicates channeling down the right third of the fracture. Assuming that the position of the latex microspheres delineates the path of least resistance for fluid as well as for colloidal particles, the fluid moving most quickly through the core enters along the upstream fracture opening and is then channeled towards the right side of the fracture. Less than 1 part in 10^4 of the injected microspheres were recovered following elution of 18 mL of carrier fluid ($\sim$ 1100 fracture volumes).

Transport of U and Np

Approximately 5 mL of 2×10^{-6} M U, and 17 mL of 2×10^{-6} M Np were injected into the core at 1 mL/hr followed by $\sim$ 300 mL of carrier solution (Table 2). Despite close to 1.5×10^3 fracture volumes of radionuclide-spiked fluid passing the core with a residence time on the order of 1 minute, no activity was detected in the effluent. Apparently, U and Np were sorbed and/or precipitated rapidly, near the fracture surface.

In an attempt to facilitate Np transport, suspensions of Np-bearing colloids derived from concrete were injected into the core in two tests (Table 2). A total of 23 mL of 2×10^{-6} M Np with colloids were eluted with 90 mL of carrier fluid. As for the soluble Np tests, no Np was detected in the effluent. Although LBS analysis could not be used to quantify the colloids passing through the core, breakthrough curves for the suspension tests indicate decreasing particle concentrations in the effluent for each successive test (Fig. 4d). The decrease in height and breadth of the breakthrough with each successive suspension test suggests the development of a filter. The fibrous alteration phases shown in SEM photos (Figs. 3a,b) are 2–5 times longer than the estimated fracture aperture height of 6 μm, and may have effectively strained the injected colloids.

Location of immobilized U and Np

A gamma counting survey of the outer core and fracture surfaces revealed high concentrations of radionuclides on the inlet face of the core. The location of immobilized radionuclides within the core was determined more precisely using alpha particle tracking and SIMS (Fig. 2). The extent and distribution of alpha particle tracks along the fracture surface was similar to that of the latex microspheres (Figs. 2a,b). This correlation confirms the hypothesis that the microspheres define the primary flow path and further suggests that radionuclides were not completely immobilized on the upstream face of the core, but were also present in the fluid moving through the fracture. In almost all cases, alpha tracks were concentrated along the fracture surface, however, in at least one case, tracks were observed several millimeters into the matrix

(Fig. 2c). Because all isotopes used in the experiment (^{238}U, ^{232}U, ^{237}Np) emit alpha particles, we were not able to determine locations of specific isotopes within the clusters of tracks.

A single SIMS transect normal to the fracture surface (Figs. 2d,e) (parallel to the upstream face, 50–75 μm into the core) recorded background levels of ^{238}U and ^{237}Np near the fracture surface and maxima several millimeters into the matrix. The breadth of the maxima, and the distance of the centroid of the maxima from the fracture surface differ for U and Np. Whether these differences reflect differences in chemistry between these two nuclides, or the fact that U and Np were eluted into the core separately, is not known. Almost all of the alpha particle tracks were localized at the fracture surface, a distribution consistent with the high K_d's observed for U and Np [1]. Hence, it is unlikely that diffusion of U and Np through the matrix explains the concentration maxima observed using SIMS. However, alpha particle tracks are observed 1–2 cm into the core along the main fracture surface (Fig. 4a), which indicates significant advective transport. This observation suggests that the U and Np recorded by the SIMS transect reflects the advective transport of U and Np via a secondary fracture that intersected either the front face of the core or the main fracture. To clarify the mechanisms that control the distribution of these radionuclides, more extensive and detailed two-dimensional maps of their concentration adjacent to the fractures are required.

Interaction of U and Np with concrete

Because U and Np were not detected in the effluent, their detection limits (Table 2) define an upper limit to the solubility of U- and Np-bearing phases that could potentially control transport. Using as input the composition of the effluent (Table 3), and assuming oxidizing conditions, and that dissolved carbonate is controlled by equilibrium with calcite, geochemical modeling calculations (with the GEMBOCHS thermodynamic database as modified by Zhao *et al.* [1]) indicate that there is only one U-bearing phase ($CaUO_4$), and no Np-bearing phases that can account for U and/or Np concentrations at or below their detection limits.

In contrast to the fracture flow experiments, U concentrations in batch experiments using the identical hydrothermally altered concrete at pH 11 [1] were 1–2 orders of magnitude greater than the detection limit. Zhao *et al.* [1] concluded that U levels were at least partly controlled by solubility, not by $CaUO_4$, but perhaps by a more soluble phase having a similar stoichiometry [16], or by solid-solution with calcite [17, 18]. A significant difference between the batch tests and the fracture flow experiment, is the ratio of Np or U to the mass of concrete. The ratio of Np or U to concrete in the flow tests would depend on the fraction of the core contacted by the tracer solution. For example, this ratio would range from several hundred to several tens of thousands of times smaller than the ratio in the batch experiments for 1% and 100% of the core contacted by the injected solution, respectively. Considering the large K_d's observed by Zhao *et al.* [1], retardation due to sorption would be expected to effectively maintain effluent concentrations well below solubility levels and detection limits even for flow paths contacting only a small fraction of the core. The presence of alpha tracks several cm into the core indicates significant transport of U and/or Np, and therefore, that only a small fraction of the core was contacted by the injected tracer.

Zhao *et al.* [1] also showed that 0.01 M $NaHCO_3$ at pH $\sim$ 10 reduced partitioning of U to this concrete by more than an order of magnitude. In contrast, eluting the U-loaded core with > 500 mL ($> 3 \times 10^4$ fracture volumes) of 2×10^{-3} M $NaHCO_3$ at pH 8.5 (Table 2) did not result in the elution of any detectable U. Apparently, at the lower pH and concentration of dissolved carbonate used in the fracture flow test, partitioning was not reduced sufficiently for U to be detected in the effluent. However, based on geochemical calculations, if U concentrations were controlled by $CaUO_4$ (the least soluble U-bearing phase in this system), U concentrations would have been detectable ($\sim 4 \times 10^{-6}$ M) in the effluent.

As observed for U, Np was not detected in the effluent in any of the four tests in which it was eluted (Table 2). Zhao *et al.* [1] observed Np concentrations above detection limits in batch experiments, and measured very high K_d's ($\sim 10^5$ mL g^{-1}) at pH 11. Based on the variation in soluble Np vs. pH for samples equilibrated between 21 and 133 days, Zhao *et al.* [1] concluded that Np concentrations were most likely controlled by sorption, rather than equilibrium with a solid phase.

Several sources report Np(V) sorption onto calcite and dolomite, the main constituents of the concrete aggregate. Keeney–Kennicutt and Morse [19] measured Np(V) sorption on calcite (5 m^2/L) at pH 7.8–8.2. The K_d calculated from the linear portion of the sorption isotherm was $\sim 2 \times 10^3$ mL/g for Np(V) sorption from deionized water. Brady *et al.* [20] reported sorption of Np(V) onto dolomite (2.3 m^2/L) in the pH range from 3 to 10, for contact times on the order of $\sim 1/2$ minute (i.e., similar to the residence time of the fluid in the fractured core). Brady *et al.* [20] observed an increase in K_d from < 10 to ~ 200 mL/g with increasing pH between 7 and 10; hence the K_d for Np on dolomite at pH 11 would be expected to be > 200 mL/g. Zhao *et al.* [1] also observed a significant increase in K_d between pH 9 and 11 for Np partitioning onto hydrothermally altered concrete. There are apparently no reported data for the sorption of Np on calcium silicate hydrate minerals, such as those found in the hydrothermally altered concrete. These minerals, as shown by SEM analysis, would be expected to present the largest surface area to the fluid in the fracture. If these phases exhibit even a modest ability to partition Np, they would significantly augment the sorptive capacity provided by the calcite and dolomite in the aggregate.

Although sorption appears to play the major role in controlling Np concentrations in the experiments of Zhao *et al.* [1] and ours, we cannot explicitly rule out subsequent precipitation of Np-bearing phases that are not represented in our thermodynamic data base, or the incorporation of Np into solid solutions. Zhao *et al.* [1] showed, using X-ray absorption spectroscopy, that over a period of 6 months, initially sorbed Np(V) is partially reduced ($\sim$ 50%) to Np(IV). It is not known whether this transformation is associated with development of an Np-bearing solid phase.

Conclusion

The immobilization of U and Np by hydrothermally altered concrete predicted by batch reaction experiments is confirmed in fracture flow studies. Under oxidizing conditions, the elution of U through concrete may be solubility limited; the elution of Np appears to be controlled primarily by sorption.

Because of the large ratio of surface area to solution volume, and the inherent reactivity of the minerals in the hydrothermally altered concrete, sorption and precipitation/dissolution reactions in the fracture are rapid. For the fracture properties and flow rates used in these experiments, reactions that immobilize and/or retard U and Np are not flow-rate dependent.

The growth of hydrothermal alteration products in fractures may make fractures self-sealing. Alteration mineral structures growing across fractures form effective particle filters.

If Np is primarily retarded by sorption onto calcite and dolomite, a potential improvement of the behavior of concrete can be effected by a suitable choice of aggregate.

Acknowledgment. We thank D. Phinney and I. Hutcheon for the SIMS analysis, and G. Eaton for help with the autoradiography. This work was performed under the auspices of the U.S. Department of Energy by the University of California Lawrence Livermore National Laboratory under contract No. W-7405-Eng-48. This work was partly supported by the Yucca Mountain Site Characterization Project, LLNL.

References

1. Zhao, P., Allen, P.G., Sylwester, E.R., Viani, B.E.: The partitioning of uranium and neptunium onto hydrothermally altered concrete. Radiochim. Acta (*this issue*) **88**, 729 (2000).
2. Bradbury, M.H., Van Loon, L.R.: *Cementitious Near-Field Sorption Data Bases for Performance Assessment of a L/ILW Repository in a Palfris Marl Host Rock*. 98-01. Paul Scherrer Institut. Wurenlingen and Villigen 1998.
3. Linklater, C.M. (Ed.): *A Natural Analogue Study of Cement-Buffered, Hyperalkaline Groundwaters And Their Interaction With A Repository Host Rock, Phase II S/98/003*. NIREX, Harwell, UK 1998.
4. Brachmann, A., Mihardja, S., Wruck, D.A., Palmer, C.E.A.: *Laser-induced Breakdown System for Colloid Characterization in Dilute Aqueous Suspensions*. UCRL-JC-135555. Lawrence Livermore National Laboratory. Livermore, CA 1999.
5. Eaton, G.F., Smith, D.K.: Aged nuclear explosive melt glass: Radiography and scanning electron microscope analyses documenting both radionuclide distribution and glass alteration. pp. 29–43. In: *Hydrologic Resources Management Program and Underground Test Area FY 1998 Progress Report*. (Smith, D.K., Eaton, G.F. eds.) UCRL-ID-135170. Lawrence Livermore National Laboratory. Livermore, CA 94550 (1999).
6. Phinney, D.L., Ryerson, F.J., Oversby, V.M., Lanford, W.A., Aines, R.D., Bates, J.K.: Integrated testing of the SRL-165 glass waste form. MRS Symposium Proceedings: Scientific Basis for Nuclear Waste Management. Vol. 84. Boston, MA. Materials Research Society 1987, pp. 433–446.
7. McKeegan, K.D., Phinney, D., Oversby, V.M., Buchholtz ten Brink, M., Smith, D.K.: Uranium transport in Topopah Spring tuff: An ion-microscope investigation. MRS Symposium Proceedings: Scientific Basis for Nuclear Waste Management. Vol. 127. Boston, MA. Materials Research Society 1989, pp. 813–821.
8. Bethke, C.M.: *The Geochemists Workbench, Release 3.0, A Users Guide to Rxn, Act2, Tact, React, and Gtplot*. Copyright Craig M. Bethke, Hydrogeology Program, University of Illinois, Champaign, IL 1998.
9. Johnson, J., Lundeen, S.: *GEMBOCHS Thermodynamic Datafiles For Use With the EQ3/6 Software Package*. Yucca Mountain Project Milestone Report M0L72. Lawrence Livermore National Laboratory. Livermore, CA 94505 (1994).
10. Chou, L., Garrels, R.M., Wollast, R.: Comparative study of the kinetics and mechanisms of dissolution of carbonate minerals. Chemical Geology **78**, 269 (1989).
11. Davis, S.N., Thompson, G.M., Bentley, H.W., Stiles, G.: Groundwater tracers – Short review. Ground Water **18**, 14 (1980).
12. Atkins, M., Glasser, F.P.: Encapsulation of radioiodine in cementitious waste forms. MRS Symposium Proceedings: Scientific Basis for Nuclear Waste Management. Vol. 176. Boston, MA. Materials Research Society 1990, pp. 15–22.
13. Heath, T.G., Ilett, D.J., Tweed, C.J.: Thermodynamic modelling of the sorption of radioelements onto cementitious materials. MRS Symposium Proceedings: Scientific Basis for Nuclear Waste Management XIX. Vol. 412. Boston. MA. Materials Research Society 1996, pp. 443–449.
14. Baker, S., McCrohon, R., Oliver, P., Pilkington, N.J.: The sorption of niobium, tin, iodine, and chlorine onto NIREX reference vault backfill. MRS Symposium Proceedings: Scientific Basis for Nuclear Waste Management. Vol. 333. Boston, MA. Materials Research Society 1994, pp. 719–724.
15. Viani, B.E., Carman, M.L.: *Transport of Soluble Species Through Tuff Core*. UCRL-ID 129183. Lawrence Livermore National Laboratory. Livermore, CA 1997.
16. Atkins, M., Glasser, F.P., Moroni, L.P.: The long-term properties of cement and concretes. MRS Symposium Proceedings: Scientific Basis for Nuclear Waste Management XV. Vol. 212. Boston, MA. Materials Research Society 1992, pp. 373–386.
17. Meece, D.E., Benninger, L.K.: The coprecipitation of Pu and other radionuclides with $CaCO_3$. Geochimica et Cosmochimica Acta **57**, 1447 (1993).
18. Curti, E.: Coprecipitation of radionuclides with calcite: estimation of partition coefficients based on a review of laboratory investigations and geochemical data. Appl. Geochem. **14**, 433 (1999).
19. Keeney-Kennicutt, W.L., Morse, J.W.: The interaction of $Np(V)O_2^+$ with common mineral surfaces in dilute aqueous solutions and seawater. Marine Chemistry **15**, 133 (1984).
20. Brady, P.V., Papenguth, H.W., Kelly, J.W.: Metal sorption to dolomite surfaces. Appl. Geochem. **14**, 569 (1999).